Low Dose Hyperoxia Primes Airways for Fibrosis in Mice after Influenza A Infection

Andrew M. Dylag[1*], Jeannie Haak[1], Rachel Warren[2], Min Yee[1], Gloria S. Pryhuber[1] and Michael A. O'Reilly[1]

[1]Department of Pediatrics, University of Rochester Medical Center, Rochester, New York, USA;

[2]Department of Microbiology and Immunology, University of Rochester Medical Center, Rochester, New York, USA

Running Title: Neonatal Hyperoxia and Airway Disease

Corresponding Author:

Andrew Dylag, MD, FAAP
Division of Neonatology, Department of Pediatrics
Golisano Children's Hospital
University of Rochester Medical Center
601 Elmwood Avenue, Box 651
Rochester, NY 14642
Phone: 585-275-5948
Fax: 585-461-3614
Email: andrew_dylag@urmc.rochester.edu
ORCID: 0000-0001-5085-5873

Statement of Financial Support: Supported by a grant from the Strong Children's Research Center at the University of Rochester and National Institutes of Health grant R01 HL091968 (MOR). NIH Center Grant P30 ES001247 supported the animal inhalation facility and the tissue-processing core. The human subject studies were supported by NHLBI Molecular Atlas of Lung Development Program Human Tissue Core grant U01HL122700 and U01HL148861 (G.H. Deutsch, T.J. Mariani, G.S. Pryhuber).
Disclosure Statement: The authors have no financial conflicts to disclose and have agreed to submission of this article.

Category of study: Basic Science
Key words: Influenza A, neonatal hyperoxia, airway hyperreactivity

Abstract: 247 words

Manuscript (not including figure legends): 4542

Abstract

It is well known that supplemental oxygen used to treat preterm infants in respiratory distress is associated with permanently disrupting lung development and the host response to influenza A virus (IAV). However, many infants who go home with normally functioning lungs are also at risk for hyperreactivity after a respiratory viral infection suggesting neonatal oxygen may have induced hidden molecular changes that may prime to the lung for disease. We discovered that thrombospondin-1 (TSP-1) is elevated in adult mice exposed to high-dose neonatal hyperoxia that is known to cause alveolar simplification and fibrotic lung disease following IAV infection. TSP-1 was also elevated in a new, low-dose hyperoxia mouse model (40% for 8 days; 40x8) that we recently reported causes a transient change in lung function that resolves by 8 weeks of age. Elevated TSP-1 was also identified in human autopsy samples of BPD-affected former preterm infants. Consistent with TSP-1 being a master TGFβ regulator, an early transient activation of TGFβ signaling, increased airway hyperreactivity, and peribronchial inflammation and fibrosis were seen when 40x8 mice were infected with IAV, which was not seen in infected room air controls. These findings reveal low dose of neonatal hyperoxia that does not affect lung function or structure may still change expression of genes, such as TSP-1, that may prime the lung for disease following respiratory viral infections, and may help explain why former preterm infants who have normal lung function are susceptible to airway obstruction and increased morbidity after viral infection.

INTRODUCTION

It is well accepted that early oxygen (O_2) exposure in preterm infants can disrupt lung development and function in extremely low gestational age newborns (ELGANs, <29 weeks gestation), often resulting in Bronchopulmonary Dysplasia (BPD). Cumulative O_2 exposure strongly predicts BPD diagnoses and severity, but approximately 40% of ELGANs escape the BPD "label" because they are weaned off O_2 or respiratory support by 36 weeks' corrected age despite having significant supplemental O_2 exposure (29, 60). Former ELGANs *with and without* BPD experience increased morbidity that can be linked to cumulative O_2 exposure with increased health care utilization, symptomatic airway disease, and asthma medication use (18, 43, 57). Former ELGANs are especially vulnerable to respiratory viral infections with increased early childhood hospitalizations for respiratory illnesses (12, 24, 51) through poorly understood mechanisms. Infection-related lung injury results in airway remodeling and longer-term airway hyperreactivity (AHR) (26, 36, 46, 65), despite increased prescriptions for asthma-related medications (53, 54). The airway dysfunction is *not* bronchodilator responsive, distinguishing it from asthma (23). Thus, there is an urgent need to uncover novel mechanisms responsible for airway dysfunction and wheezing in former ELGANs.

Neonatal hyperoxia is one of the most commonly used exposures in animal models to perturb lung development and model BPD (10). Mice are born in the saccular stage of lung development where airways continue developing and alveolar structure is in its primitive stages, analogous to ELGANs (4). The dose and duration of hyperoxia matters when modeling neonatal O_2 exposure in mice. For example, multiple studies, including several from our own laboratory, show that severe hyperoxia ($\geq$ 60% O_2 for $\geq$ 4 days) creates a BPD-like phenotype (10, 63) with alveolar simplification, airway remodeling, and viral susceptibility (14, 25, 35, 38, 40, 41, 44, 49, 67), even after a long period of room air recovery. These previous models, however, are limited because they often use O_2 doses higher than those seen in real-world NICU settings and cause such profound alveolar simplification that it is difficult to discern physiological changes in the airway. This led our laboratory to develop a translational model of low dose chronic hyperoxia (40% O_2 for 8 days; 40x8) which causes transiently increased airway resistance and decreased lung compliance with AHR and airway smooth muscle hypertrophy at 4 weeks (21), consistent with other studies (61). Interestingly, abnormal lung function, AHR, and

47 smooth muscle hypertrophy all resolve at 8 weeks (21), where mice are morphologically and
48 functionally "normal." Taken together, our model of lower O_2 exposures in preterm infants in modern
49 NICUs shows changes in airway function without overt signs of alveolar simplification. We suggest this
50 may more accurately replicate preterm infants with increased respiratory morbidity after leaving the
51 NICU without a diagnosis of BPD.

52 Neonatal hyperoxia also has functional implications when adult mice are challenged with
53 Influenza A viral (IAV) infection. Previous studies by our laboratory have shown that adult IAV infected
54 who received higher dose neonatal hyperoxia (100% for 4 days, 100x4) at birth experience persistent
55 inflammation and parenchymal fibrosis (14, 25, 35, 40, 41, 67). We previously showed that 100x4
56 hyperoxia depletes cardiomyocytes in the lung which has implications on pulmonary hypertension.
57 Secondary analysis of that dataset suggests hyperoxia stimulates extracellular matrix thrombospondin
58 1 (TSP-1) and several members of the A Disintegrin and Metalloproteinase with Thrombospondin
59 motifs (ADAMTS) family of proteinases which have TSP-1 like activity. Since TSP-1 upregulates TGFβ
60 activity, we hypothesized that 40x8 adult mice would be primed for increased fibrosis after IAV
61 infection. Herein, we show that when challenged with the HKx31 H3N2 Influenza A Virus (IAV) adult
62 40x8 mice develop peribronchial fibrosis after infection not observed in room air (RA) controls, that
63 pathologically resolves over time, but persistently decreases lung compliance, thus creating a model of
64 transient morbidity.

METHODS

Animal Exposures and Infection. All protocols were approved by the Institutional Animal Care and Use Committee of University of Rochester (Rochester, NY) and were consistent with The Association for Assessment and Accreditation of Laboratory Animal Care International policies (Frederick, MD). Litters of C57Bl/6J (Jackson Laboratory, Bar Harbor, ME) were placed into room air (RA) or 40% oxygen from post-natal day (PND) 0-8 as previously described (21). Nursing dams were rotated every 24-48 hours. After exposure, pups were allowed to mature until PND 56 under room air conditions where a subset of naïve mice were harvested for pulmonary function or qRT-PCR analysis. Infected mice were lightly anesthetized with ketamine/xylazine mixture and given 10^5 plaque forming units (PFUs) influenza A (x31/H3N2) virus, which was grown and titered in Madin-Darby Canine Kidney (MCDK) cells as previously described (64). Mice were weighed every other day for two weeks after infection, then weekly thereafter.

Bronchoalveolar Lavage. Bronchoalveolar lavage (BAL) was performed in a subset of animals at post-infection day (PID) 3, 7, 10, and 14 with 3 separate 1 mL aliquots of ice-cold phosphate-buffered saline (PBS, FisherScientific, Hampton, NH), as previously described (14). The first supernatant was collected for protein analysis and frozen at -80˚C for further analysis.

Cell differentiation. BAL Fluid (BALF) from all 3 aliquots were combined, then separated by centrifugation with removal of erythrocytes in ammonium chloride lysing solution (0.15 M NH_4Cl, 10 mM $NaHCO_3$, 1 mM EDTA). Total cell count was measured with a TC20 Automated Cell counter (Bio-Rad, Hercules, CA). BALF was then transferred onto slides with a cytological centrifuge (Shandon Cytospin 2, Runcorn, UK) and stained with a Hema 3 Stain Set (FisherScientific, Hampton, NH). Images of stained cells were taken with a Nikon E800 microscope (Nikon Instruments Inc., Melville, NY) using a SPOT RT3 Camera and SPOT Imaging Software (v5.2, Diagnostic Instruments, Inc., Sterling Heights, MI). At least 200 cells were counted per slide with ImageJ (NIH, Bethesda, MD). Macrophages/monocytes, neutrophils, and lymphocytes were individually enumerated by two separate investigators.

Protein analysis. BALF was analyzed using a DuoSet ELISA kit for Mouse CCL2/JE/MCP-1 and TGF-β1 (R&D Systems, Minneapolis, MN) according to the manufacturer's instructions using a

SpectraMax M5 Microplate Reader (Molecular Devices, San Jose, CA) and Softmax Pro 6.4 (Molecular Devices). The detection range for this assay was 3.9-250 pg/mL. Additionally, latent TGF-β1 was activated by incubating samples with 1N HCl and neutralizing with 1.2 N NaOH/0.5 M HEPES, as per kit instructions, and another ELISA performed to measure immunoreactive TGF-β1.

Pulmonary Function Testing. Naïve (8-10 weeks old) and IAV-infected (14 and 56 days post-infection) mice were anesthetized with a ketamine/xylazine mixture [100 mg/kg (Par Pharmaceutical, Chestnut Ridge, NY) and 20 mg/kg (Acorn, Inc., Lake Forest, IL), respectively], immobilized with pancuronium bromide (10 mg/kg, Sigma-Aldrich, St. Louis, MO), and ventilated (SCIREQ Inc., Montreal, Canada) with a tidal volume of 10 ml/kg, 150 breaths/min, PEEP of 3 cm H_2O, and FIO_2 of 21% as previously described (21). Respiratory system resistance (R_{rs}), Newtonian airway resistance (R_N), respiratory system compliance (C_{rs}), Elastance (H), Tissue Damping (G), hysteresivity (η, eta) were measured in triplicate at both time points.

Human Tissues. Donor lungs samples were provided through the federal United Network of Organ Sharing via National Disease Research Interchange (NDRI) and International Institute for Advancement of Medicine (IIAM) and entered into the NHLBI LungMAP Biorepository for Investigations of Diseases of the Lung (BRINDL) at the University of Rochester Medical Center overseen by the IRB as RSRB00047606, as previously described (5, 7). Lung tissue sections were uniformly obtained from the right lower lobe of 6 infants, 3 infants born prematurely (25, 26, and 28 gestational weeks) that died between 84 and 86 weeks post-menstrual age with BPD (2 ventilator dependent, died of respiratory failure, 1 with chronic lung disease, but not vent dependent died of accidental event) and 3 infants, each born full term and died at 74 to 100 weeks post-menstrual age of other non-pulmonary causes (n = 3 in each group). No acute viral infections were reported in the past medical history of any infant. Sections (5 µm) of formalin inflated, paraffin embedded RLL parenchymal lung tissue blocks were de-paraffinized, re-hydrated, and stained for Anti-Thrombospondin 1 (ab85762, abcam, Cambridge, UK) and DAPI Fluoromount-G (SouthernBiotech, Birmingham, AL).

Immunohistochemistry. At PIDs 14 and 56, right lobes of lungs were snap-frozen for qRT-PCR, and left lobes perfused with 10% neutral buffered formalin (NBF, Fisher Scientific, Hampton, NH) at 25 mm/Hg, embedded in paraffin wax, and cut to 4 µm thick. Additional samples were taken after saline

flush with 1x PBS, before perfusion with NBF. Lung slices were stained with Hematoxylin and Rubens Eosin-Phloxine (H&E; Biocare Medical, Concord, CA) and Gomori's Trichrome (Richard-Allan Scientific, San Diego, CA) for collagen.

Fluorescent immunohistochemistry was performed with primary antibodies S100A4 (FSP-1) (1:1000, PA5-82322, ThermoFisher Scientific, Waltham, MA), Anti-Influenza A Virus Nucleoprotein (NP; NR-43899, BEI Resources, Manassas, VA) or Anti-Thrombospondin 1 (ab85762, abcam, Cambridge, UK), with secondary antibody AlexaFluor 594 (1:200, A21207, ThermoFisher Scientific) and DAPI Fluoromount-G counterstain to view activated macrophages. Stained images were taken with a Nikon E800 microscope (Nikon Instruments Inc., Melville, NY) using a SPOT RT3 Camera and SPOT Imaging Software (v5.2, Diagnostic Instruments, Inc., Sterling Heights, MI). Photographs were analyzed with ImageJ.

Fibroblast and collagen staining. FSP1 and Sirius red staining were quantified using ImageJ. Fluorescent images of each airway were taken under red (FSPI, Sirius red) and blue (DAPI) channels. A threshold for each fluorescence was set, and the same used for all images taken. Airway perimeter was measured to ensure only small airways analyzed, then enlarged by 40 (Sirius red) and 80 µm (FSP1). Particle area (Sirius red) and number (FSP1) were measured, to determine their prevalence surrounding the airways.

qRT-PCR. RNA was extracted from tissue with TRIzol Reagent (Invitrogen, Carlsbad, CA) as previously described (69). Complimentary DNA was run on a C1000 ThermoCycler (Bio-Rad) using a Maxima First Strand cDNA Synthesis Kit (ThermoScientific). Quantitative real-time PCR was performed using iQ SYBR Green Supermix (Bio-Rad) with CFX96 Real-Time System (Bio-Rad). Genes of interest where run on plates with *mGapdh* as housekeeping gene, and analyzed using the $\Delta\Delta C_T$ method (33). Three to four samples per treatment were run in duplicate on each plate. Primer sequences can be found in Table 1.

Statistical Analysis. Statistical analyses were performed in GraphPad Prism (GraphPad Software v8, San Diego, CA). Pulmonary function data was subjected to D'Agostino & Pearson and Shapiro-Wilk tests for normality, Brown-Forsythe test for variance, and ordinary one-way ANOVA with Tukey's multiple comparisons test for significance. In instances of failed normality or variance, Kruskal-Wallis non-parametic and Dunn's multiple comparisons tests were performed for significance. Weight over time was tested for normality and variance, as described above, and multiple t-tests performed with Holm-Sidak correction. Cell differentiation data and ELISA data was subjected to Shapiro-Wilk test for normality. Holm-Sidak correction for multiple comparisons was used to further test cell differentiation and Kruskal-Wallis non-parametic and Dunn's multiple comparisons tests were performed for significance on ELISA data. qRT-PCR data was analyzed using the $\Delta\Delta C_T$ method, and graphed as fold-change normalized to RA = 1. *P* values of ≤ 0.05 were considered significant for all analyses performed, and values graphed as mean ± SEM.

Results

Molecular differences persist in low-dose hyperoxia-exposed mice after Room Air Recovery

RA and 40x8 uninfected (naïve) mice were recovered in room air until 8-10 weeks of age (PND56, Figure 1A). We confirmed that RA and 40x8 animals have similar alveolar and airway structure by histology (Figure 1B), consistent with our laboratory's previously published study (21). Furthermore, pulmonary function, measurements were similar between RA and 40x8 adult mice at this time point (Figure 1C). To determine whether adult RA and recovered 40x8 lungs had similar gene expression, we examined a previously published Affymetrix array in adult mice who received high-dose (100x4 oxygen at birth for candidate genes (68). Out of 45,109 probes present on the array, 54 transcripts were differentially expressed between the RA and the 100x4 mice using a false discovery rate of 10%. Neonatal hyperoxia reduced expression of 43 genes, most of which reflected a loss of pulmonary cardiomyocytes (68). We analyzed the upregulated transcripts for genes regulating inflammation using qRT-PCR and found the extracellular matrix protein thrombospondin 1 (TSP-1) and several members of the A Disintegrin and Metalloproteinase with Thrombospondin motifs (ADAMTS) family of proteinases were upregulated in the high dose 100x4 model (Figure 1D). TSP-1 and ADAMTS share common functions in their ability to activate latent TGFβ through conformational change of the latent binding protein that opens the binding site of TGFβ to its receptor (16). We confirmed that TSP-1 expression is increased 40x8 in adult mice and did not detect increased ADAMTS proteinases at high enough levels to justify further study (Figure 1D), thus choosing to focus on TSP-1.

TSP-1 expression is increased in hyperoxia-exposed mice and humans with BPD

To evaluate the prevalence and distribution of TSP-1, tissue sections of naïve 40x8 mice and BPD-affected human tissue samples were stained with TSP-1 antibody and counterstained with DAPI. In 40x8 mice, TSP-1 was increased in the alveolar spaces (Figure 2A) but less noticeable around the airways. In humans (N=3 controls, N=3 BPD lungs), increased TSP-1 was similarly detected in the alveolar spaces of 2/3 BPD infants where staining was much more sparse in control infants (Figure *2B*).

TGFβ signaling is altered in adult animals exposed to neonatal hyperoxia

To determine if key TGFβ signaling pathway mediators were different between RA and 40x8 animals, qRT-PCR was performed on naïve RA and 40x8 adult mice. We did not observe increased *expression of TGF*β-R1, or any of the canonical SMAD genes (Figures 3A, D, E, and F). Conversely, there was a strong trend for decreased *Tgfb-R2* and *Tgfb-R3* in naïve mice before infection (Figures 3B, C).

Oxygen Exposed Mice Have Worse Airway Disease after Influenza Infection

Since TSP-1 activates TGFβ, we wanted to test the hypothesis that the 40x8 lung was primed to activate TGFβ signaling following an insult. We administered IAV to hyperoxia and RA exposed mice as a profibrotic challenge, because IAV causes fibrosis in mice and hyperoxia-exposed infants have increased morbidity after viral infections. To test this hypothesis, adult RA (RA-PBS or RA-x31) and 40x8 (O_2-PBS or O_2-x31) mice were nasally inoculated with HKx31 IAV or sham (PBS) (Figure 4A). Infection was confirmed by positive nucleoprotein (NP) staining in the airway club cells, indicating active IAV infection in both RA-x31 and O2-x31 animals (Figure 4B). Two weeks after infection, persistent airway inflammation (Figure 4C) and fibrosis (Figure 4D) were observed in O_2-treated animals compared to RA controls. To confirm increased fibrosis in O_2-x31 animals, Sirius Red collagen staining was performed (Figure 4E), imaged, and quantified in both groups with a focus on the peribronchial spaces. Again, we observed increased Sirius Red staining (Figure 4F) in 40x8 animals 2 weeks post-infection. Weight loss over the first two post-infection weeks were not different between the RA-x31 and O2-x31 groups during the first two post-infection weeks through 8 weeks post-infection, whereas sham animals appropriately did not lose weight (Figure 4G). There were no differences in weight loss between male and female mice (data not shown). The observed histologic changes resolved by 8 weeks post-infection (Figure 4H).

Comprehensive assessments of pulmonary function were performed at both 2 and 8 weeks post infection to determine if the observed histologic findings had a physiologic correlate. At two weeks post infection, 40x8 animals had higher total Respiratory System Resistance (R_{rs}, Figure 5A), Newtonian Airway Resistance (R_N, Figure 5B), and Elastance (H, Figure 5E) with decreased Respiratory System Compliance (C_{rs}, Figure 5C). Tissue damping (G, Figure 5D) and hysteresivity (eta, Figure 5F) were

unchanged. The magnitude of the changes in R_N (which contributes to R_{rs}) signify the majority of resistance change is due to changes in airway resistance. Interestingly, at 8 weeks post infection, the resistance changes normalized (Figures 5A-B), whereas the compliance and elastance (Figures 5C, 5E) remained persistently abnormal in the 40x8 animals where the RA animals returned to their previous levels. This suggests that lung function has reached a new, lower physiologic baseline, even after a long period of room-air recovery.

Oxygen Exposed Mice have Persistent Peribronchial Inflammation

We next sought to determine whether low dose O_2 exposure is associated with increased inflammatory cells similar to our previous studies using high-dose (100x4) oxygen (39). Bronchoalveolar Lavage Fluid (BALF) was obtained, spun, and quantified with differential cell counts at 4 time points during infection: days 3, 7, 10, and 14. Though we found a slight increase in total cell counts and neutrophils 7 days post infection in RA-x31 animals (Figure 6A-B), cell counts were otherwise similar between groups at the 3, 7, and 10 day time points. However, O_2-x31 animals had trends for increased total and macrophage cell counts, 14 days after infection (Figure 6A, 6D). Quantification of MCP-1 protein was similar at all time points during infection (data not shown), distinguishing it from other studies in our laboratory (13), indicating that there may be alternate mechanisms driving increased inflammation in this model. To better characterize the inflammatory cells present around the airways, tissue sections were stained for fibroblast stimulatory protein 1 (FSP1), a marker shown to identify inflammatory subpopulations of macrophages (42). Increased FSP1 staining was concentrated around the small airways at 14 days post infection (Figure 6F) and was detected more frequently in O_2-x31 animals (Figure 6G). Notably, FSP-1 staining was almost absent in the alveolar spaces with no differences detected between RA-x31 and O_2-x31 animals (data not shown).

The histologic, physiologic, and phenotypic differences in 40x8 animals led us to investigate possible mechanisms by which increased inflammation and fibrosis would be present and drive increased pulmonary morbidity after IAV infection. We analyzed BAL fluid for TGFβ using ELISA and observed a strong trend for increased active/total TGFβ 3 days post infection that normalized by 7 days (Figure 6E).

DISCUSSION

Airway disease in former ELGANs is characterized by increased airflow obstruction in infancy (31), specifically in the mid-to-later forced expiratory flows (47, 52). These functional deficits predispose ELGANs to wheezing in infancy and childhood irrespective of their BPD status (8, 9, 15, 27, 28, 32, 56). Since BPD is often defined by need for supplemental O_2 near term corrected gestational age (60), many infants who were exposed to O_2 escape the BPD diagnosis, but still have significant pulmonary morbidity associated with their extreme prematurity. Our laboratory has performed several clinical studies quantifying cumulative O_2 exposure in ELGANs *with and without BPD* and have shown that ELGANs with increased O_2 exposure have worse obstructive lung disease ($FEV_{0.5}$/FVC ratio), but "high" and "low" O_2 exposed ELGANs have significant airflow obstruction (FEF_{75}) compared to term infants at 1-year of age (22). Those functional studies were performed in asymptomatic, well ex-preterm infants, but there is an abundance of evidence that when challenged with a respiratory infection, former ELGANs have more significant lower airway symptoms with wheezing suggesting airflow obstruction and increased rehospitalization rates (20, 55, 65). These clinical studies emphasize that there is a spectrum of lung disease present in former ELGANs, and thus justifies studying a spectrum of O_2 exposures in the laboratory that more closely model variant neonatal exposures, focusing on airway pathology to determine their impacts on lung development, function, and response to infection.

Using these ELGAN studies, we sought to create a translationally relevant paradigm of low-dose neonatal hyperoxia to show that mice are primed for airway disease when challenged with respiratory viral infection in adulthood. We chose 40% oxygen for 8 days because our previous studies showed that 40x8 mice have transiently increased airway hyperreactivity at 4 weeks of age that resolves by 8 weeks, such that the recovered animal is functionally and phenotypically indistinguishable from RA controls. This distinguishes it from other models wherein prolonged high O_2 concentrations cause significant alveolar simplification, making it difficult to discern and isolate differences in airway pathology. Relatively low-dose 40x8 oxygen does not cause significant alveolar simplification, though if left in 40% oxygen for longer periods subtle changes in alveolar structure are detectable (37). We wanted to test if the "repaired" lung after hyperoxia would respond similarly to a RA animal when challenged with influenza A virus and hypothesized based on other studies from our laboratory (14, 25,

35, 40, 41, 67) that there would be persistently altered response to IAV, even after a long period of RA recovery. We chose HKx31 strain of influenza because it causes lower-airway symptoms, usually without mortality, and mice respond to IAV similarly compared to humans (19, 30, 58); unlike some other viruses (e.g. Respiratory Syncytial Virus) more commonly seen in infants that are difficult to model in mice. Our model is robust such that it recapitulates several observations in former ELGANs: 1) O_2 causes changes in baseline airway mechanics, 2) airway changes are not overwhelmed by alveolar simplification, and 3) O_2 exposed mice show increased severity of disease with viral infection. Additionally, many hyperoxia mouse models administer virus right when animals come out of hyperoxia, whereas this model allows for RA recovery and post-hyperoxia lung repair. Our 40x8 infection model occurs long after cessation of oxygen exposure, which has translational strengths to reflect former ELGANs later in infancy. Finally, other published models of airway dysfunction often treat animals with allergen or methacholine to observe differences in AHR. While this has been useful in identifying changes in airway smooth muscle, it may not explain airway disease of prematurity because these children often spontaneously wheeze following viral infections yet medications targeting airway smooth muscle relaxation (bronchodilators) are most often ineffective. Similarly, our infection-related changes are evident at baseline and without methacholine, implicating alternate mechanisms of airway pathology in O_2 exposed mice apart from smooth muscle bronchospasm, distinguishing it from asthma.

We showed that 40x8 mice have increased airway-specific fibrotic repair resulting in hyperactive airways, associated with TGFβ hyperactivation, and delayed inflammatory resolution compared to room air controls. Our laboratory previously established a mouse model of high-dose neonatal hyperoxia (100% x 4 days; 100x4) followed by adult IAV infection associated with increased MCP1, marked *alveolar parenchymal fibrosis*, and increased mortality. In this paradigm, 100x4 mice have interstitial fibrosis, enhanced epithelial cell death, and increased mortality when exposed to IAV as adults (14, 25, 35, 40, 41, 67). These changes were partially attributed to the loss of type II alveolar epithelial cells (AEC2s) (69), but since 40x8 hyperoxia does not cause loss of AEC2s, other mechanisms driving disease severity were considered. IAV infection of 40x8 mice using the same virus increased morbidity, and was associated with peribronchial fibrosis 2 weeks after infection not observed in RA controls. Pulmonary function was abnormal with increased resistance and elastance and

297 decreased compliance. We observed delayed clearance of immune cells 2 weeks after infection with
298 increased staining for activated macrophages (fibroblast-specific protein 1, FSP-1 (42)) in 40x8 animals
299 and trends for increased total and macrophage cell count in bronchoalveolar lavage fluid at that time
300 point. IAV infection in 40x8 mice was not associated with increased weight loss or monocyte
301 chemoattractant protein-1 (MCP-1) (13) (data not shown) as previously reported. Finally, 8 weeks after
302 infection, the resistance changes resolve leaving behind subtle significant changes in compliance,
303 establishing a model of intermittent morbidity that causes a downward shift in baseline lung function
304 after infection in O_2-x31 animals.

305 The peribronchial fibrosis changes in our model are associated with TGFβ hyperactivation. The
306 TGFβ pathway regulates normal alveolar lung development (71). Global/floxed knockouts of TGFβ or
307 key pathway mediators results in impaired alveolarization (50), but its role in airway development is
308 more poorly defined. TGFβ1 signals through the canonical SMAD and/or non-SMAD dependent
309 pathways to regulate gene expression, which in the lung can promote ECM collagen deposition and
310 remodeling. The TGFβ signaling machinery changes both its expression and localization within the lung
311 across developmental stages. Notably, TGFβ-R1 (receptor 1, ALK5), TGFβ-R2 (receptor 2), and
312 SMAD3 decrease in expression throughout development, but change localization from vessels to
313 airways as mice age such that when alveolarization is complete very little staining is evident in the
314 alveolar spaces (3). This same study demonstrated that similar processes occur during human
315 development, with most staining evident in the airways or vascular smooth muscle layer for ALK1,
316 TGFβ-R1/ALK5, TGFβ-R2, and SMAD2. The evolutionary reason behind these changes throughout
317 development have not been fully established, but may be concentrated in the areas of greatest lung
318 growth during alveolarization. Dysregulation of the TGFβ pathway and its machinery has been
319 implicated in hyperoxia-induced lung injury (2, 59, 66). Specifically, higher dose (85% O_2 x 28 days)
320 hyperoxia leads to a 4-fold increase and relocalization of the TGF-β2 receptor to the airway epithelium
321 (2). Similarly, hyperoxia leads to a 6-fold increase co-SMAD/SMAD4 staining, also notable in the airway
322 epithelium and alveolar septae (2). However, whole lung expression of these TGFβ pathway
323 components in adult mice after 40x8 hyperoxia, was not increased, which led us to further investigate
324 TSP-1 as a protein of interest.

Our finding of increased TSP-1 may provide mechanistic insight into IAV-related morbidity in hyperoxia exposed mice and humans with BPD. TSP-1 is a calcium binding ECM glycoprotein first discovered in platelet granules (6) and later localized to many other tissues including the lung (1). TSP-1 is synthesized by endothelial cells, fibroblasts, smooth muscle cells, monocytes, and macrophages (34) and interacts with several ECM components including integrins, fibronectin, cell receptors, growth factors (like TGFβ-1), cytokines, and proteases (11, 45). Antiangiogenesis, smooth muscle proliferation, nitric oxide signaling antagonism, and inflammation regulation are known functions of TSP-1 relevant to the lung (1). TSP-1 is required to form normal airway epithelium, as TSP1-null animals have bronchial epithelial hyperplasia, proximal mucous metaplasia, vascular smooth muscle hyperplasia, club cell hyperplasia, and uncontrolled inflammation (16). In contrast, upregulation of TSP-1 was noted in the preterm ventilated lung on autopsy (17), an in utero model of tracheal occlusion (62) (lung stretch), and other profibrotic diseases, but to our knowledge this has not been further explored in BPD. The BPD model is of particular interest because TSP-1 may play a role in capillary rarefication (also seen in mouse hyperoxia models (70)) and contribute to other hyperoxia-induced diseases such as pulmonary hypertension (48). Indeed, we confirmed increased alveolar staining for TSP-1 in both 40x8 exposed adult mice and BPD-affected human infants. The balanced regulation of TGFβ is vital for survival as TSP1-null and TGFβ-1-null mice both die of similar phenotypes (pneumonia) within weeks of birth (16). The strikingly similar phenotype of TSP1-null and TGFβ-1-null mice suggest that TSP-1 is the main TGFβ activator *in vivo* (16). Together, these previous studies on TSP-1/TGFβ create a potential “dual priming” effect of neonatal hyperoxia on the airway by the following mechanisms: 1) TGFβ receptor and signaling molecules localize to the airway throughout development and/or during hyperoxia exposure and 2) increased TSP-1 is primed to hyperactivate TGFβ. Thus, TSP-1 is an intriguing candidate for further study in rodent BPD models and in the extremely preterm infant.

Our results suggest low-dose neonatal O_2 causes “silent” changes in gene expression with long-term functional consequences after a lung insult such as respiratory viral infection, and that the “repaired” lung still reacts abnormally to a profibrotic stimulus such as IAV. This 40x8 hyperoxia model causes an airway-specific phenotype observed at baseline and drives increased respiratory morbidity after infection, thus recapitulating airway diseases observed in former ELGANs. We can now exploit

this model to better understand the origins of TGFβ hyperactivation (including TSP-1 as a candidate protein), and determine its source and specificity for the viral responses that may explain infection related morbidity in vulnerable former ELGANs.

Acknowledgments

The authors would like to acknowledge Ethan David Cohen for his technical assistance and advice regarding the manuscript, and thank Biorepository for Investigation of Neonatal Diseases of the Lung (BRINDL) part of the Clinical and Translational Science Institute Informatics, Research Data Integration and Analytics group, University of Rochester Medical Center, for human tissue samples.

We are extremely grateful to the families who have generously given precious gifts to support this research. We thank the members of the LungMAP Consortium for their collaborations and the members of the Pryhuber lab (Amanda Howell, Heidie Huyck, and Cory Poole) who prepared the human lung tissue.

Author Contributions

AMD conceived the study and designed experiments. AMD and JH performed experiments with assistance from MY and RW. AMD and JH interpreted the data and wrote the manuscript. GSP curated the human tissue samples, and revised the manuscript. MOR conceived the study, revised the manuscript. All authors approved of the final version.

Statement of Financial Support

Supported by a grant from the Strong Children's Research Center at the University of Rochester and National Institutes of Health grant R01 HL091968 (MOR). NIH Center Grant P30 ES001247 supported the animal inhalation facility and the tissue-processing core. The human subject studies were supported by NHLBI Molecular Atlas of Lung Development Program Human Tissue Core grant U01HL122700 and U01HL148861 (G.H. Deutsch, T.J. Mariani, G.S. Pryhuber).

Disclosure

The authors declare that no conflict of interest exists.

References

1. **Adams JC, and Lawler J**. The thrombospondins. *Cold Spring Harb Perspect Biol* 3: a009712, 2011.
2. **Alejandre-Alcazar MA, Kwapiszewska G, Reiss I, Amarie OV, Marsh LM, Sevilla-Perez J, Wygrecka M, Eul B, Kobrich S, Hesse M, Schermuly RT, Seeger W, Eickelberg O, and Morty RE**. Hyperoxia modulates TGF-beta/BMP signaling in a mouse model of bronchopulmonary dysplasia. *Am J Physiol Lung Cell Mol Physiol* 292: L537-549, 2007.
3. **Alejandre-Alcazar MA, Michiels-Corsten M, Vicencio AG, Reiss I, Ryu J, de Krijger RR, Haddad GG, Tibboel D, Seeger W, Eickelberg O, and Morty RE**. TGF-beta signaling is dynamically regulated during the alveolarization of rodent and human lungs. *Dev Dyn* 237: 259-269, 2008.
4. **Amy RW, Bowes D, Burri PH, Haines J, and Thurlbeck WM**. Postnatal growth of the mouse lung. *J Anat* 124: 131-151, 1977.
5. **Ardini-Poleske ME, Clark RF, Ansong C, Carson JP, Corley RA, Deutsch GH, Hagood JS, Kaminski N, Mariani TJ, Potter SS, Pryhuber GS, Warburton D, Whitsett JA, Palmer SM, Ambalavanan N, and Lung MAPC**. LungMAP: The Molecular Atlas of Lung Development Program. *American journal of physiology Lung cellular and molecular physiology* 313: L733-L740, 2017.
6. **Baenziger NL, Brodie GN, and Majerus PW**. A thrombin-sensitive protein of human platelet membranes. *Proc Natl Acad Sci U S A* 68: 240-243, 1971.
7. **Bandyopadhyay G, Huyck HL, Misra RS, Bhattacharya S, Wang Q, Mereness J, Lillis J, Myers JR, Ashton J, Bushnell T, Cochran M, Holden-Wiltse J, Katzman P, Deutsch G, Whitsett JA, Xu Y, Mariani TJ, and Pryhuber GS**. Dissociation, cellular isolation, and initial molecular characterization of neonatal and pediatric human lung tissues. *American journal of physiology Lung cellular and molecular physiology* 315: L576-L583, 2018.
8. **Baraldi E, Carraro S, and Filippone M**. Bronchopulmonary dysplasia: Definitions and long-term respiratory outcome. *Early Hum Dev* 85: S1-S3, 2009.
9. **Been JV, Lugtenberg MJ, Smets E, van Schayck CP, Kramer BW, Mommers M, and Sheikh A**. Preterm birth and childhood wheezing disorders: a systematic review and meta-analysis. *PLoS Med* 11: e1001596, 2014.
10. **Berger J, and Bhandari V**. Animal models of bronchopulmonary dysplasia. The term mouse models. *Am J Physiol-Lung C* 307: L936-L947, 2014.
11. **Bornstein P**. Diversity of function is inherent in matricellular proteins: an appraisal of thrombospondin 1. *J Cell Biol* 130: 503-506, 1995.
12. **Broughton S, Roberts A, Fox G, Pollina E, Zuckerman M, Chaudhry S, and Greenough A**. Prospective study of healthcare utilisation and respiratory morbidity due to RSV infection in prematurely born infants. *Thorax* 60: 1039-1044, 2005.
13. **Buczynski BW, Yee M, Martin KC, Lawrence BP, and O'Reilly MA**. Neonatal hyperoxia alters the host response to influenza A virus infection in adult mice through multiple pathways. *American journal of physiology Lung cellular and molecular physiology* 305: L282-290, 2013.
14. **Buczynski BW, Yee M, Martin KC, Lawrence BP, and O'Reilly MA**. Neonatal hyperoxia alters the host response to influenza A virus infection in adult mice through multiple pathways. *Am J Physiol-Lung C* 305: L282-L290, 2013.
15. **Colin AA, McEvoy C, and Castile RG**. Respiratory morbidity and lung function in preterm infants of 32 to 36 weeks' gestational age. *Pediatrics* 126: 115-128, 2010.
16. **Crawford SE, Stellmach V, Murphy-Ullrich JE, Ribeiro SM, Lawler J, Hynes RO, Boivin GP, and Bouck N**. Thrombospondin-1 is a major activator of TGF-beta1 in vivo. *Cell* 93: 1159-1170, 1998.
17. **De Paepe ME, Greco D, and Mao Q**. Angiogenesis-related gene expression profiling in ventilated preterm human lungs. *Exp Lung Res* 36: 399-410, 2010.

18. **Di Fiore JM, Dylag AM, Honomichl RD, Hibbs AM, Martin RJ, Tatsuoka C, and Raffay TM**. Early inspired oxygen and intermittent hypoxemic events in extremely premature infants are associated with asthma medication use at 2 years of age. *J Perinatol* 39: 203-211, 2019.
19. **Doherty PC, Topham DJ, and Tripp RA**. Analysing the T cell response to influenza viruses in mouse model systems. *Int Congr Ser* 1123: 153-165, 1996.
20. **Doyle LW, Ford G, and Davis N**. Health and hospitalistions after discharge in extremely low birth weight infants. *Semin Neonatol* 8: 137-145, 2003.
21. **Dylag AM, Haak J, Yee M, and O'Reilly MA**. Pulmonary mechanics and structural lung development after neonatal hyperoxia in mice. *Pediatr Res* 2019.
22. **Dylag AM, Kopin HG, O'Reilly MA, Wang H, Davis SD, Ren CL, and Pryhuber GS**. Early Neonatal Oxygen Exposure Predicts Pulmonary Morbidity and Functional Deficits at One Year. *J Pediatr* 2020. Accepted.
23. **Filippone M, Carraro S, and Baraldi E**. The term "asthma" should be avoided in describing the chronic pulmonary disease of prematurity. *The European respiratory journal* 42: 1430-1431, 2013.
24. **Furman L, Baley J, Borawski-Clark E, Aucott S, and Hack M**. Hospitalization as a measure of morbidity among very low birth weight infants with chronic lung disease. *J Pediatr* 128: 447-452, 1996.
25. **Giannandrea M, Yee M, O'Reilly MA, and Lawrence BP**. Memory CD8(+) T Cells Are Sufficient To Alleviate Impaired Host Resistance to Influenza A Virus Infection Caused by Neonatal Oxygen Supplementation. *Clin Vaccine Immunol* 19: 1432-1441, 2012.
26. **Gien J, and Kinsella JP**. Pathogenesis and treatment of bronchopulmonary dysplasia. *Curr Opin Pediatr* 23: 305-313, 2011.
27. **Greenough A**. Long-term pulmonary outcome in the preterm infant. *Neonatology* 93: 324-327, 2008.
28. **Halvorsen T, Skadberg BT, Eide GE, Roksund O, Aksnes L, and Oymar K**. Characteristics of asthma and airway hyper-responsiveness after premature birth. *Pediatric allergy and immunology : official publication of the European Society of Pediatric Allergy and Immunology* 16: 487-494, 2005.
29. **Higgins RD, Jobe AH, Koso-Thomas M, Bancalari E, Viscardi RM, Hartert TV, Ryan RM, Kallapur SG, Steinhorn RH, Konduri GG, Davis SD, Thebaud B, Clyman RI, Collaco JM, Martin CR, Woods JC, Finer NN, and Raju TNK**. Bronchopulmonary Dysplasia: Executive Summary of a Workshop. *J Pediatr* 197: 300-308, 2018.
30. **Hikono H, Kohlmeier JE, Ely KH, Scott I, Roberts AD, Blackman MA, and Woodland DL**. T-cell memory and recall responses to respiratory virus infections. *Immunol Rev* 211: 119-132, 2006.
31. **Hoo AF, Gupta A, Lum S, Costeloe KL, Huertas-Ceballos A, Marlow N, and Stocks J**. Impact of ethnicity and extreme prematurity on infant pulmonary function. *Pediatric pulmonology* 49: 679-687, 2014.
32. **Kotecha SJ, Edwards MO, Watkins WJ, Henderson AJ, Paranjothy S, Dunstan FD, and Kotecha S**. Effect of preterm birth on later FEV1: a systematic review and meta-analysis. *Thorax* 68: 760-766, 2013.
33. **Livak KJ, and Schmittgen TD**. Analysis of relative gene expression data using real-time quantitative PCR and the 2(-Delta Delta C(T)) Method. *Methods* 25: 402-408, 2001.
34. **Lopez-Dee Z, Pidcock K, and Gutierrez LS**. Thrombospondin-1: multiple paths to inflammation. *Mediators Inflamm* 2011: 296069, 2011.
35. **Maduekwe ET, Buczynski BW, Yee M, Rangasamy T, Stevens TP, Lawrence BP, and O'Reilly MA**. Cumulative Neonatal Oxygen Exposure Predicts Response of Adult Mice Infected With Influenza A Virus. *Pediatr Pulm* 50: 222-230, 2015.
36. **Maitre NL, Ballard RA, Ellenberg JH, Davis SD, Greenberg JM, Hamvas A, Pryhuber GS, Prematurity, and Respiratory Outcomes P**. Respiratory consequences of prematurity: evolution of a diagnosis and development of a comprehensive approach. *J Perinatol* 35: 313-321, 2015.
37. **Nardiello C, Mizikova I, Silva DM, Ruiz-Camp J, Mayer K, Vadasz I, Herold S, Seeger W, and Morty RE**. Standardisation of oxygen exposure in the development of mouse models for bronchopulmonary dysplasia. *Dis Model Mech* 10: 185-196, 2017.

38. **O'Reilly M, Harding R, and Sozo F**. Altered small airways in aged mice following neonatal exposure to hyperoxic gas. *Neonatology* 105: 39-45, 2014.
39. **O'Reilly MA, Marr SH, Yee M, McGrath-Morrow SA, and Lawrence BP**. Neonatal hyperoxia enhances the inflammatory response in adult mice infected with influenza A virus. *American journal of respiratory and critical care medicine* 177: 1103-1110, 2008.
40. **O'Reilly MA, Marr SH, Yee M, McGrath-Morrow SA, and Lawrence BP**. Neonatal hyperoxia enhances the inflammatory response in adult mice infected with influenza A virus. *Am J Resp Crit Care* 177: 1103-1110, 2008.
41. **O'Reilly MA, Yee M, Buczynski BW, Vitiello PF, Keng PC, Welle SL, Finkelstein JN, Dean DA, and Lawrence BP**. Neonatal Oxygen Increases Sensitivity to Influenza A Virus Infection in Adult Mice by Suppressing Epithelial Expression of Ear1. *Am J Pathol* 181: 441-451, 2012.
42. **Osterreicher CH, Penz-Osterreicher M, Grivennikov SI, Guma M, Koltsova EK, Datz C, Sasik R, Hardiman G, Karin M, and Brenner DA**. Fibroblast-specific protein 1 identifies an inflammatory subpopulation of macrophages in the liver. *Proc Natl Acad Sci U S A* 108: 308-313, 2011.
43. **Raffay TM, Dylag AM, Sattar A, Abu Jawdeh EG, Cao S, Pax BM, Loparo KA, Martin RJ, and Di Fiore JM**. Neonatal intermittent hypoxemia events are associated with diagnosis of bronchopulmonary dysplasia at 36 weeks postmenstrual age. *Pediatric research* 85: 318-323, 2019.
44. **Regal JF, Lawrence BP, Johnson AC, Lojovich SJ, and O'Reilly MA**. Neonatal oxygen exposure alters airway hyperresponsiveness but not the response to allergen challenge in adult mice. *Pediat Allerg Imm-Uk* 25: 180-186, 2014.
45. **Resovi A, Pinessi D, Chiorino G, and Taraboletti G**. Current understanding of the thrombospondin-1 interactome. *Matrix Biol* 37: 83-91, 2014.
46. **Reyburn B, Martin RJ, Prakash YS, and MacFarlane PM**. Mechanisms of injury to the preterm lung and airway: implications for long-term pulmonary outcome. *Neonatology* 101: 345-352, 2012.
47. **Robin B, Kim YJ, Huth J, Klocksieben J, Torres M, Tepper RS, Castile RG, Solway J, Hershenson MB, and Goldstein-Filbrun A**. Pulmonary function in bronchopulmonary dysplasia. *Pediatric pulmonology* 37: 236-242, 2004.
48. **Rogers NM, Ghimire K, Calzada MJ, and Isenberg JS**. Matricellular protein thrombospondin-1 in pulmonary hypertension: multiple pathways to disease. *Cardiovasc Res* 113: 858-868, 2017.
49. **Royce SG, Nold MF, Bui C, Donovan C, Lam M, Lamanna E, Rudloff I, Bourke JE, and Nold-Petry CA**. Airway Remodeling and Hyperreactivity in a Model of Bronchopulmonary Dysplasia and Their Modulation by IL-1 Receptor Antagonist. *Am J Resp Cell Mol* 55: 858-868, 2016.
50. **Saito A, Horie M, and Nagase T**. TGF-beta Signaling in Lung Health and Disease. *Int J Mol Sci* 19: 2018.
51. **Sampalis JS**. Morbidity and mortality after RSV-associated hospitalizations among premature Canadian infants. *J Pediatr* 143: S150-156, 2003.
52. **Sanchez-Solis M, Garcia-Marcos L, Bosch-Gimenez V, Perez-Fernandez V, Pastor-Vivero MD, and Mondejar-Lopez P**. Lung function among infants born preterm, with or without bronchopulmonary dysplasia. *Pediatric pulmonology* 47: 674-681, 2012.
53. **Slaughter JL, Stenger MR, Reagan PB, and Jadcherla SR**. Inhaled bronchodilator use for infants with bronchopulmonary dysplasia. *Journal of Perinatology* 35: 61-66, 2015.
54. **Slaughter JL, Stenger MR, Reagan PB, and Jadcherla SR**. Utilization of inhaled corticosteroids for infants with bronchopulmonary dysplasia. *PloS one* 9: e106838, 2014.
55. **Smith VC, Zupancic JAF, McCormick MC, Croen LA, Greene J, Escobar GJ, and Richardson DK**. Rehospitalization in the first year of life among infants with bronchopulmonary dysplasia. *J Pediatr-Us* 144: 799-803, 2004.
56. **Speer CP, and Silverman M**. Issues relating to children born prematurely. *Eur Respir J Suppl* 27: 13s-16s, 1998.

57. **Stevens TP, Dylag A, Panthagani I, Pryhuber G, and Halterman J**. Effect of cumulative oxygen exposure on respiratory symptoms during infancy among VLBW infants without bronchopulmonary dysplasia. *Pediatric pulmonology* 45: 371-379, 2010.
58. **Van Reeth K**. Cytokines in the pathogenesis of influenza. *Vet Microbiol* 74: 109-116, 2000.
59. **Vyas-Read S, Wang WY, Kato S, Colvocoresses-Dodds J, Fifadara NH, Gauthier TW, Helms MN, Carlton DP, and Brown LAS**. Hyperoxia induces alveolar epithelial-to-mesenchymal cell transition. *Am J Physiol-Lung C* 306: L326-L340, 2014.
60. **Walsh MC, Yao Q, Gettner P, Hale E, Collins M, Hensman A, Everette R, Peters N, Miller N, Muran G, Auten K, Newman N, Rowan G, Grisby C, Arnell K, Miller L, Ball B, McDavid G, National Institute of Child H, and Human Development Neonatal Research N**. Impact of a physiologic definition on bronchopulmonary dysplasia rates. *Pediatrics* 114: 1305-1311, 2004.
61. **Wang H, Jafri A, Martin RJ, Nnanabu J, Farver C, Prakash YS, and MacFarlane PM**. Severity of neonatal hyperoxia determines structural and functional changes in developing mouse airway. *Am J Physiol-Lung C* 307: L295-L301, 2014.
62. **Warburton D, and Kaartinen V**. When the lung is stretched, could it be thrombospondin via TGFbeta1 peptide activation? *J Physiol* 584: 365, 2007.
63. **Warner BB, Stuart LA, Papes RA, and Wispe JR**. Functional and pathological effects of prolonged hyperoxia in neonatal mice. *Am J Physiol-Lung C* 275: L110-L117, 1998.
64. **Warren R, Domm W, Yee M, Campbell A, Malone J, Wright T, Mayer-Proschel M, and O'Reilly MA**. Ataxia-telangiectasia mutated is required for the development of protective immune memory after influenza A virus infection. *Am J Physiol Lung Cell Mol Physiol* 317: L591-L601, 2019.
65. **Weisman LE**. Populations at risk for developing respiratory syncytial virus and risk factors for respiratory syncytial virus severity: infants with predisposing conditions. *Pediatr Infect Dis J* 22: S33-37; discussion S37-39, 2003.
66. **Yang HP, Fu JH, Xue XD, Yao L, Qiao L, Hou A, Jin LL, and Xing YJ**. Epithelial-Mesenchymal Transitions in Bronchopulmonary Dysplasia of Newborn Rats. *Pediatr Pulm* 49: 1112-1123, 2014.
67. **Yee M, Buczynski BW, Lawrence BP, and O'Reilly MA**. Neonatal Hyperoxia Increases Sensitivity of Adult Mice to Bleomycin-Induced Lung Fibrosis. *Am J Resp Cell Mol* 48: 258-266, 2013.
68. **Yee M, Cohen ED, Domm W, Porter GA, Jr., McDavid AN, and O'Reilly MA**. Neonatal hyperoxia depletes pulmonary vein cardiomyocytes in adult mice via mitochondrial oxidation. *Am J Physiol Lung Cell Mol Physiol* 314: L846-L859, 2018.
69. **Yee M, Gelein R, Mariani TJ, Lawrence BP, and O'Reilly MA**. The Oxygen Environment at Birth Specifies the Population of Alveolar Epithelial Stem Cells in the Adult Lung. *Stem cells (Dayton, Ohio)* 34: 1396-1406, 2016.
70. **Yee M, White RJ, Awad HA, Bates WA, McGrath-Morrow SA, and O'Reilly MA**. Neonatal hyperoxia causes pulmonary vascular disease and shortens life span in aging mice. *Am J Pathol* 178: 2601-2610, 2011.
71. **Zhao L, Yee M, and O'Reilly MA**. Transdifferentiation of alveolar epithelial type II to type I cells is controlled by opposing TGF-beta and BMP signaling. *Am J Physiol Lung Cell Mol Physiol* 305: L409-418, 2013.

574 **Figure Legends**
575

576 **Figure 1.** A) Model timeline of hyperoxia exposure and recovery in naïve mice. B) H&E sections of RA
577 and hyperoxia (40% for 8 days; 40x8) exposed mice resemble RA controls at PND 56. C) Pulmonary
578 function measurements are similar between RA and 40x8 mice for Respiratory System Resistance
579 (R_{rs}), Newtonian airway resistance (R_N), Respiratory system compliance (C_{rs}), Tissue Damping (G),
580 Elastance (H), and hysteresivity (η, eta). *n* ≥ 8 per group. D) qRT-PCR of RA and 40x8 mice at PND 56
581 shows increased *Tsp1* and similar expression levels of other identified candidate genes. Data represent
582 means ± SEM. ** $p \leq 0.01$. Scale bar = 100 µm.

583

584 **Figure 2.** Lung samples were obtained from C57BL/6J A) mice at PND 56 that were exposed to oxygen
585 at PND 0-8, and B) former premature infants at 1-2 year who passed away from BPD with non-BPD
586 age-matched controls. Slides were stained with antibody to TSP-1 (red) and counterstained with DAPI
587 (blue). White arrows indicate TSP-1+ cells. *aw* = airway. N = 3 samples per group. Scale bar = 100 µm.

588

589 **Figure 3.** qRT-PCR was performed at PND 56 on naïve RA and 40x8 mice for A) TGFBRI, B)
590 TGFBRII, C) TGFBR3, D) SMAD2, E) SMAD3, and F) SMAD4/co-smad. Data represent means ± SEM;
591 *n* = 3-4 samples per group.

592

593 **Figure 4.** A) Experimental timeline for O_2 exposure and IAV exposures. At PND 56, mice previously
594 exposed to RA or 40x8 at PND 0-8, were intranasally infected with 10^5 PFU of H3N2 HKx31 IAV or
595 PBS (sham). B) Fluorescent NP (red), counterstained with CCSP (green) and DAPI (blue), at PID3
596 indicates viral infection in small airways of both treatment groups. C) H&E and D) Trichrome stains at
597 PID 14 indicate increased inflammation and fibrosis around the small airways of O_2-x31 animals. E)
598 Sirius red staining at 2 weeks post-infection shows increased collagen deposition in the O_2-x31
599 treatment group. F) Increased Sirius red staining was detected around O_2-x31 airways compared to
600 RA. G) Animals of both groups that received IAV lost significantly more weight than sham mice, but
601 similar weight loss occurred between infected groups. H) H&E staining at PID 56 showed a recovered

602 phenotype with resolved inflammation and fibrosis for both groups. Data represent means ± SEM; *n* ≥ 5
603 samples per group. Scale bars = 100 µm. PND = post-natal day, PID = post-infection day.
604
605 Figure 5. Pulmonary function testing at PID14 and 56. A) R_{rs} and B) R_N were higher in the O2-x31
606 group at PID14 indicating more hyperactive airways. C) C_{rs} was decreased in O_2-x31 animals at both
607 time points D) G was unchanged at both time points E) H was increased at both time points indicating
608 increased tissue stiffness F) η remained unchanged at both time points indicating homogenous lung
609 disease. Data represent means ± SEM; *n* ≥ 8 samples per group. * $p \leq 0.05$. R_{rs} – respiratory system
610 resistance, R_N – Newtonian resistance, C_{rs} – respiratory system compliance, G – tissue damping, H –
611 tissue elastance, η (eta) - hysteresivity.

612 Figure 6. BALF was collected at PID 3, 7, 10, and 14 from RA-x31 and O_2-x31 animals. A). Total cells,
613 B) neutrophils C) lymphocytes, and D) macrophages were enumerated. Total cells were increased in
614 the RA-x31 group at PID 7 and trends for increased total cells and macrophages were present at PID
615 14. E) ELISA was performed to determine ratio of activated/total TGF-β1 on PIDs 3 and 7 BALF. A
616 trend towards a significant increase in O_2-x31 protein at PID 3 was seen. PID 14 lung slices were
617 stained with antibodies to FSP-1 (red) and DAPI (blue). F) More FSP-1+ cells were present around O_2-
618 x31 airways group compared to RA-x31 controls. Data represent means ± SEM; *n* ≥ 5 samples per
619 group. # $p < 0.10$ (trend), * $p \leq 0.05$, ** $p \leq 0.01$.

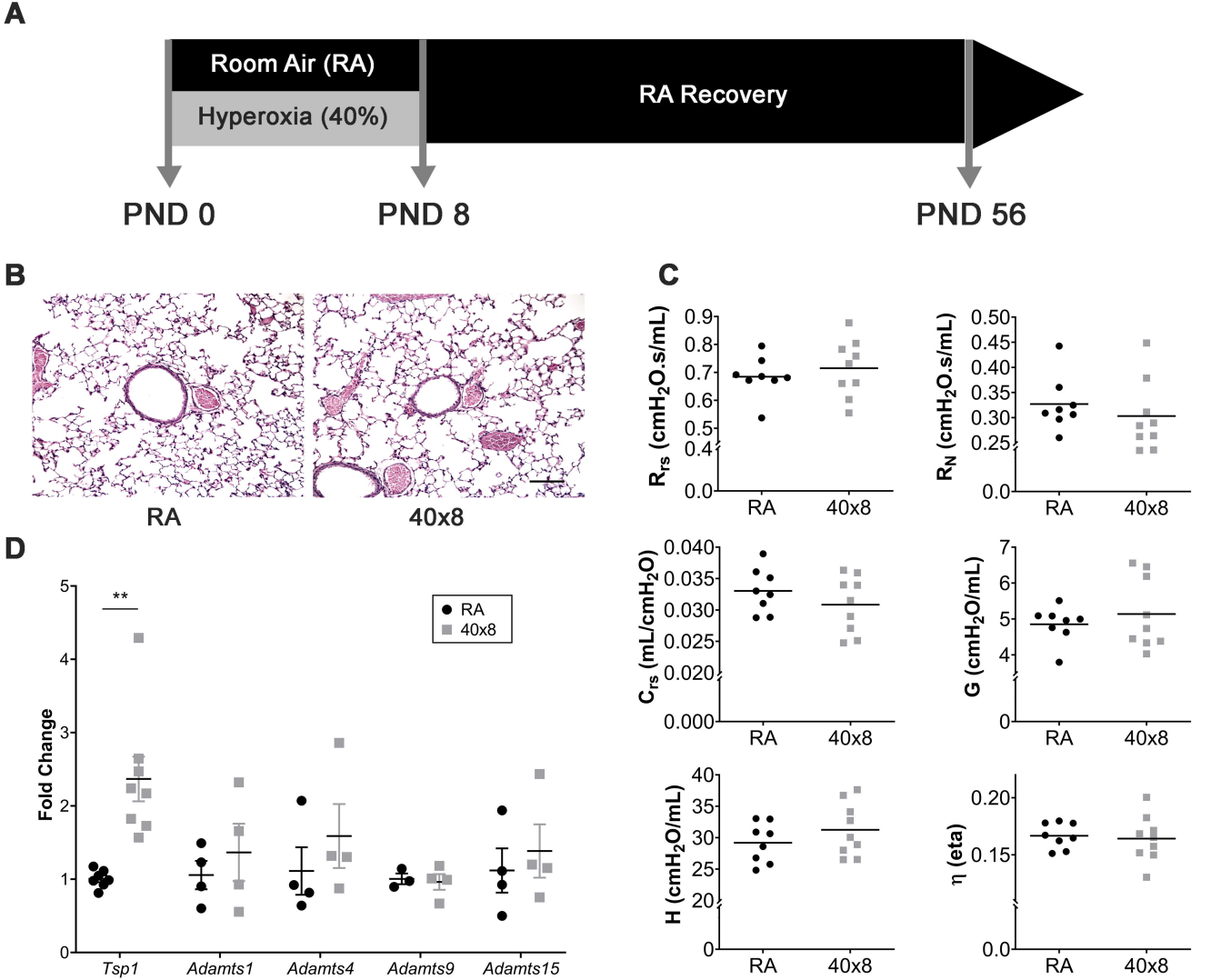
A
Room Air (RA)
Hyperoxia (40%)
RA Recovery
PND 0
PND 8
PND 56
B
RA
40x8
C
R_{rs} ($cmH_2O.s/mL$)
R_N ($cmH_2O.s/mL$)
C_{rs} (mL/cmH_2O)
G (cmH_2O/mL)
H (cmH_2O/mL)
η (eta)
RA
40x8
D
Fold Change
**
RA
40x8
Tsp1
Adamts1
Adamts4
Adamts9
Adamts15

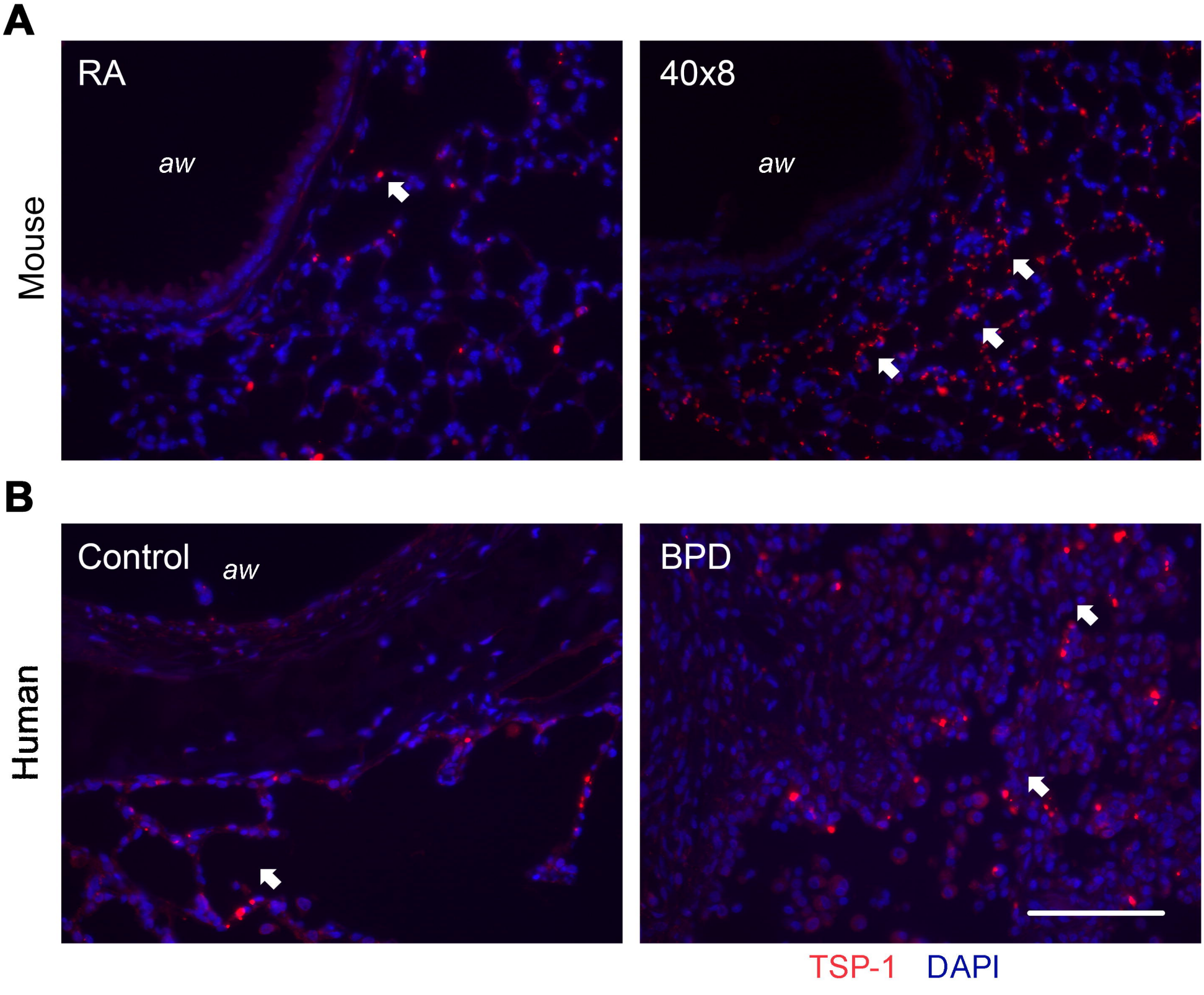
A
RA
aw
40x8
aw
Mouse
B
Control
aw
BPD
Human
TSP-1
DAPI

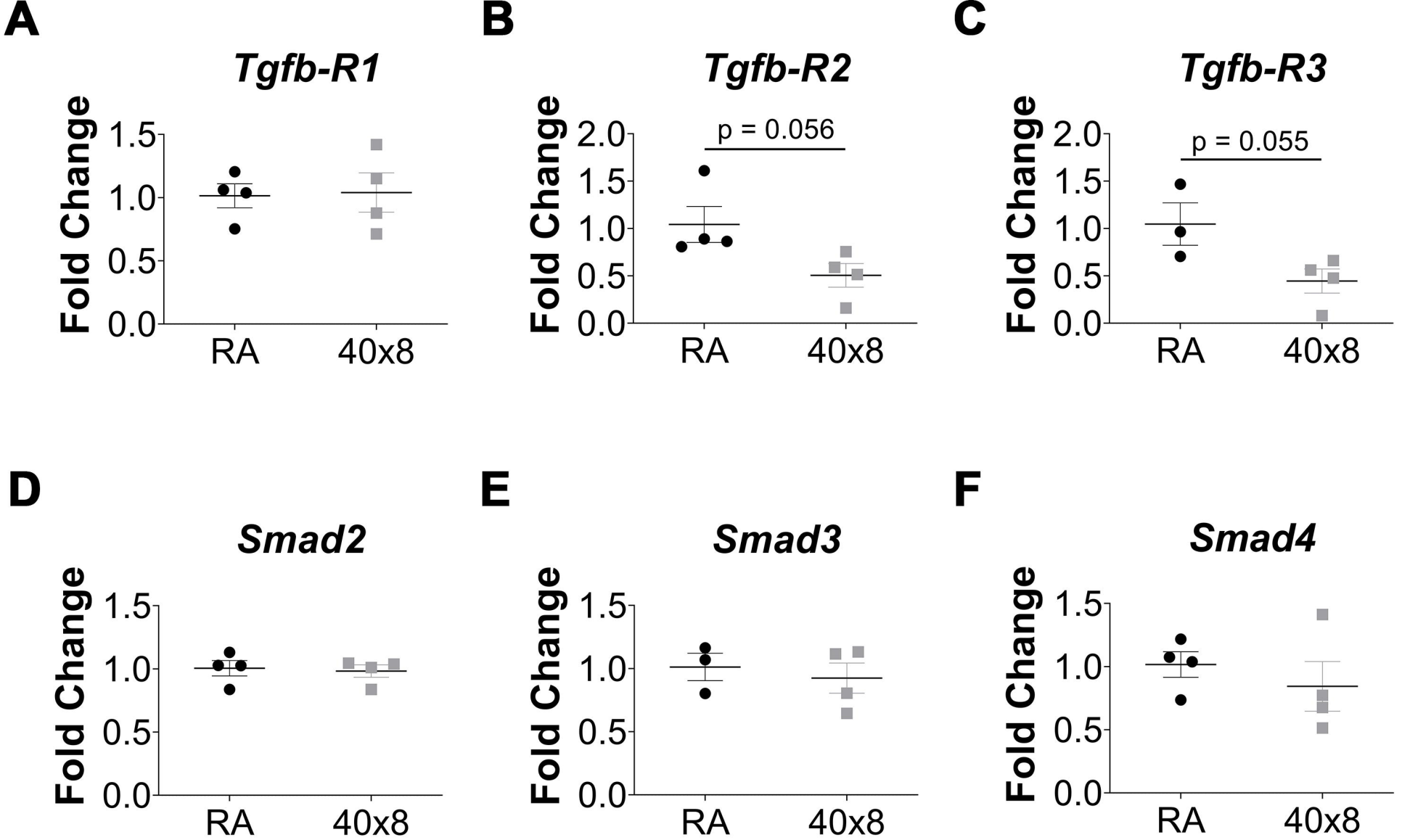
A
Tgfb-R1
Fold Change
1.5
1.0
0.5
0.0
RA
40x8
B
Tgfb-R2
p = 0.056
Fold Change
2.0
1.5
1.0
0.5
0.0
RA
40x8
C
Tgfb-R3
p = 0.055
Fold Change
2.0
1.5
1.0
0.5
0.0
RA
40x8
D
Smad2
Fold Change
1.5
1.0
0.5
0.0
RA
40x8
E
Smad3
Fold Change
1.5
1.0
0.5
0.0
RA
40x8
F
Smad4
Fold Change
1.5
1.0
0.5
0.0
RA
40x8

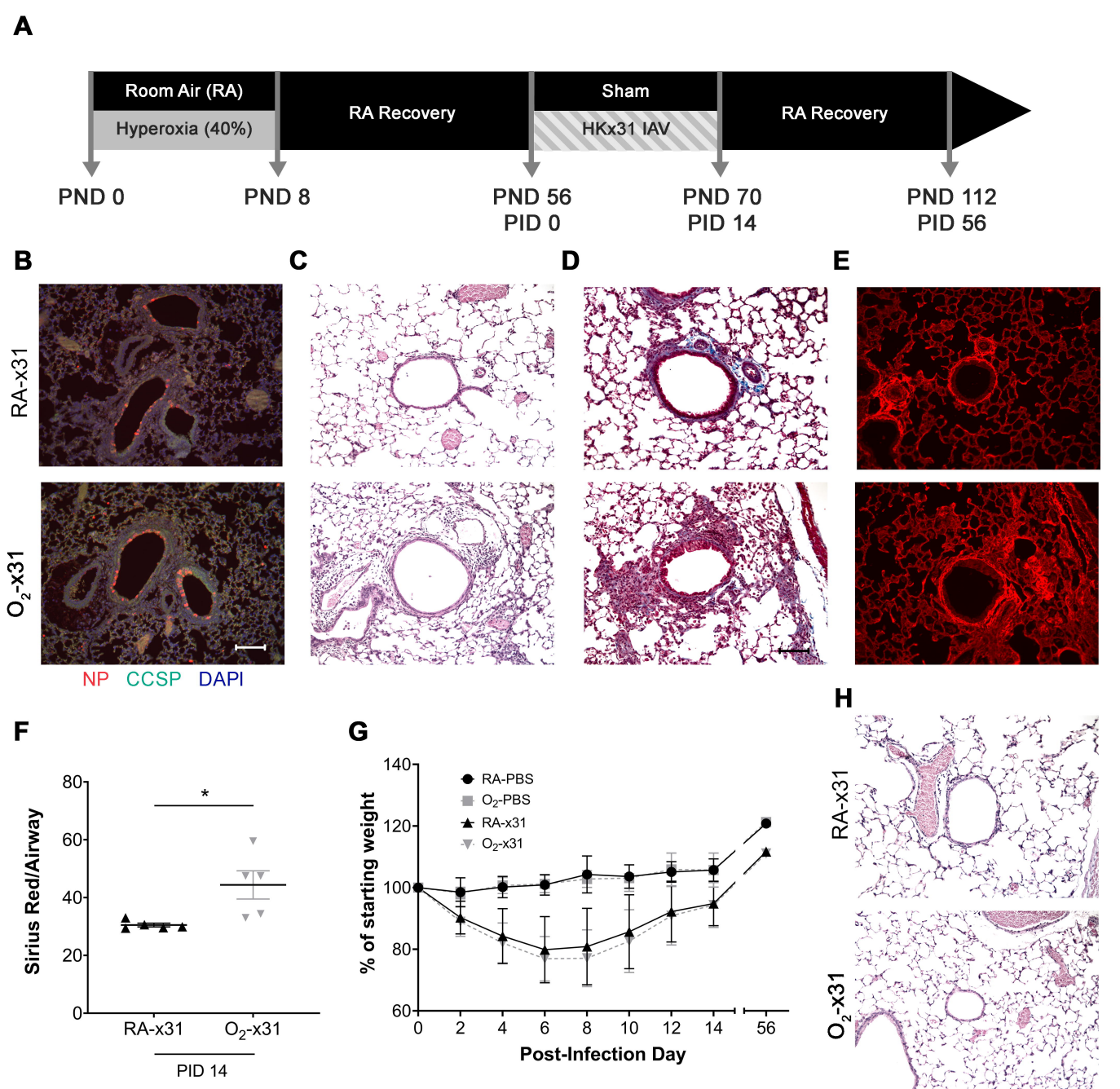
A
Room Air (RA)
Hyperoxia (40%)
RA Recovery
Sham
HKx31 IAV
RA Recovery
PND 0
PND 8
PND 56
PID 0
PND 70
PID 14
PND 112
PID 56
B
C
D
E
RA-x31
O2-x31
NP CCSP DAPI
F
Sirius Red/Airway
80
60
40
20
0
*
RA-x31
O2-x31
PID 14
G
% of starting weight
140
120
100
80
60
RA-PBS
O2-PBS
RA-x31
O2-x31
0 2 4 6 8 10 12 14 56
Post-Infection Day
H
RA-x31
O2-x31

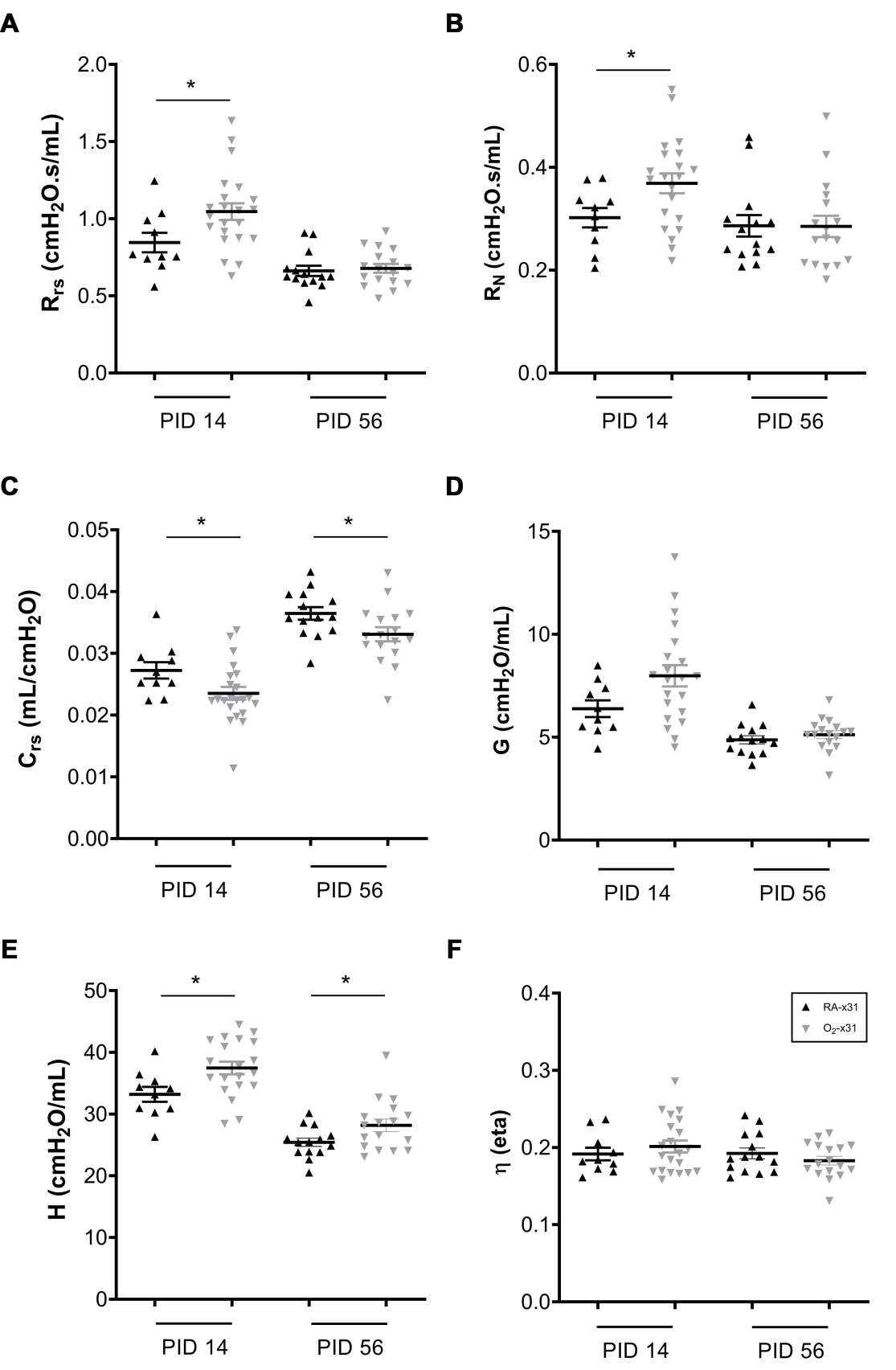
A
B
C
D
E
F
R_{rs} ($cmH_2O.s/mL$)
R_N ($cmH_2O.s/mL$)
C_{rs} (mL/cmH_2O)
G (cmH_2O/mL)
H (cmH_2O/mL)
η (eta)
PID 14
PID 56
RA-x31
O_2-x31
*

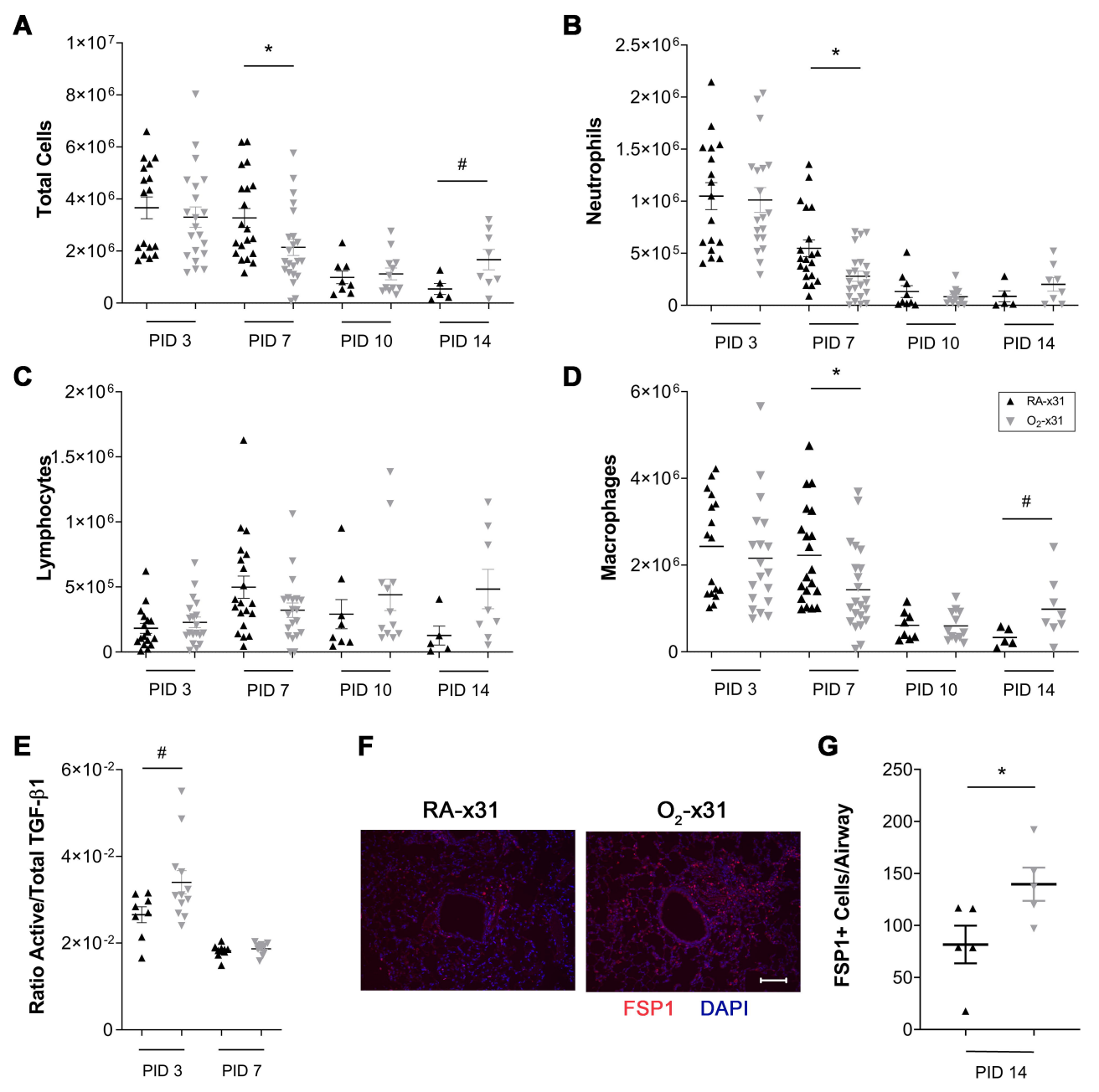
A
Total Cells
1×10^7
8×10^6
6×10^6
4×10^6
2×10^6
0
*
#
PID 3
PID 7
PID 10
PID 14
B
Neutrophils
2.5×10^6
2×10^6
1.5×10^6
1×10^6
5×10^5
0
*
PID 3
PID 7
PID 10
PID 14
C
Lymphocytes
2×10^6
1.5×10^6
1×10^6
5×10^5
0
PID 3
PID 7
PID 10
PID 14
D
Macrophages
6×10^6
4×10^6
2×10^6
0
*
#
RA-x31
O2-x31
PID 3
PID 7
PID 10
PID 14
E
Ratio Active/Total TGF-β1
6×10^-2
4×10^-2
2×10^-2
0
#
PID 3
PID 7
F
RA-x31
O2-x31
FSP1
DAPI
G
FSP1+ Cells/Airway
250
200
150
100
50
0
*
PID 14

Tables

Table 1. qRT-PCR Primer Sequences.

Primer	Forward (5' - 3')	Reverse (5' - 3')
mTsp-1	TCC CCT ATT CTG GAG GGT TC	TCC CTG GAA ATA GGC ACA AG
mAdamts1	CTC GTA GCT GAC CAG TCC AT	ACT TCT GGT CCC TTC TGC TC
mAdamts4	CAG ACG AAG CAC TCA CCT T	CCA GCC TGA GGA ACA TTG A
mAdamts9	GCC TGT GCT ACC TTA CCT AAA C	CCA CAA GTC ACG GAA CAA GAG
mAdamts15	TGA TCT GTC TCC GAC CCT CA	GAC TCA CCA TGC CCA CT
mTgfβ-R1	AAA ACA GGG GCA GTT ACT ACA AC	TGG CAG ATA TAG ACC ATC AGC A
mTgfβ-R2	AAC ATG GAA GAG TGC AAC GAT	CGT CAC TTG GAT AAT GAC CAA CA
mTgfβ-R3	GGT GTG AAC TGT CAC CGA TCA	GTT TAG GAT GTG AAC CTC CCT TG
mSmad1	ACC CCT ACC ACT ATA AGC GAG	TGC TGG AAA GAG TCT GGG AAC
mSmad2	ATG TCG TCC ATC TTG CCA TTC	AAC CGT CCT GTT TTC TTT AGC TT
mSmad3	CAC AGC CAC CAT GAA TTA CGG	TGG CGT CTC TAC TCT CTG ATA GT
mSmad4	CAT TCC AGC GTG CCA TTT C	TTC AAA GTA AGC AAT GGA GCA C
mGapdh	TGT CCG TCG TGG ATC TGA C	CCT GCT TCA CCA CCT TCT TG